

Using mobility data in the design of optimal lockdown strategies for the COVID-19 pandemic in England*

Ritabrata Dutta^{1†}, Susana Gomes², Dante Kalise³, Lorenzo Pacchiardi⁴

¹*Department of Statistics, Warwick University, UK*

²*Department of Mathematics, Warwick University, UK*

³*School of Mathematical Sciences, University of Nottingham, UK*

⁴*Department of Statistics, University of Oxford, UK*

September 8, 2021

Abstract

A mathematical model for the COVID-19 pandemic spread in England is presented. The model integrates age-structured Susceptible-Exposed-Infected-Removed dynamics with real mobile phone data accounting for the population mobility. The dynamical model adjustment is performed via Approximate Bayesian Computation. Optimal lockdown and exit strategies are determined based on nonlinear model predictive control, constrained to public-health and socio-economic factors. Through an extensive computational validation of the methodology, it is shown that it is possible to compute robust exit strategies with realistic reduced mobility values to inform public policy making.

Keywords: COVID-19, Lockdown strategy, epidemic model, SEIRD, Google mobility, Approximate Bayesian computation, Model predictive control.

1 Introduction

The COVID-19 pandemic has put quantitative decision-making methods (and the lack thereof) in the spotlight. Designing informed non-pharmaceutical intervention strategies (NPIS) to mitigate the pandemic effects has been a controversial issue worldwide. In particular, the planning of effective lockdown policies and their posterior lifting based on real-time data still remains a largely open problem. A vast amount of research efforts has been dedicated to model the COVID-19 pandemic focusing on the various aspects of the system dynamics, such as estimating the value of the basic reproductive number [Hilton and Keeling, 2020, Kucharski et al., 2020], evaluating the effect of containment measures and travel restrictions [Warne et al., 2020, Gatto et al., 2020, Kucharski et al., 2020, Prem et al., 2020, Chinazzi et al., 2020], assessing the effect of age on the transmission and severity of the disease [Davies et al., 2020, Hilton and Keeling, 2020] and estimating the impact on Health Services [IHME and Murray, 2020]. It is remarkably hard, if not impossible, to capture every aspect of this complex phenomenon in an integrated and computationally tractable mathematical model. With this in mind, our goal in the present work is to study the dynamics of COVID-19 spread in England by integrating a dynamical epidemiological model with mobile phone data from the population. Such an adjusted model yields an accurate account of the real displacement of the population between different locations (e.g. workplaces, schools, etc.) during the pandemic, and serves as the basis for determining lockdown and exit strategies which are optimised according to public health and socio-economic constraints.

Related Literature. Previous works have modelled the impact of NPIS using extensions of the classical Susceptible-Infected-Removed (SIR) model [Kermack and McKendrick, 1927] with the inclusion of compartments corresponding to asymptomatic population Exposed to infections but not infectious, and Infected

*Code is available at: <https://github.com/OptimalLockdown/MobilitySEIRD-England>

†Corresponding author: Ritabrata.Dutta@warwick.ac.uk. (Research planned by RD, LP, SG, DK; research done by LP, RD and paper written by LP, RD, SG, DK.)

infectious [Rothe et al., 2020]. Given the current knowledge of the COVID-19 disease, this constitutes a complete description of the possible states.

Among the works based on the aforementioned state space representation, Prem et al. [2020], one of the main inspirations behind our work, uses an age-structured model to quantify the effect of control measures imposed in Wuhan, China and concludes that there exists a large potential on the use of NPIs for mitigating the COVID-19 pandemic. Furthermore, the authors recommend a gradual relaxation strategy in comparison to an early lifting of the imposed lockdown measures to avoid possible second and third waves of the pandemic. Using a stochastic modification of a compartmental model without age structure, Kucharski et al. [2020] reaches similar conclusions and quantifies the effectiveness of lockdown measures by estimating the reproduction number, which decreased from a median value of 2.35 before travel restrictions were imposed, to 1.05 one week after the implementation of travel restrictions.

In the context of resorting to optimal control methods to determine a lockdown policy, Rawson et al. [2020] compares a switching on-off strategy with a two-stage release from quarantine (with part of the population released first, and the others later). The authors consider a threshold-based sanitary cost functional aiming at releasing the largest possible population without exceeding the availability of hospital beds, and their conclusion is to favour the second strategy. Charpentier et al. [2020] consider multiple control levels, such as the number of tests (both virologic and anti-body tests) and the increase of ICU beds in addition to the reduction of social contacts, and uses a cost functional involving both economic and sanitary costs. The authors suggest an optimal lockdown policy which involves a quick and strong isolation, followed by a large increase in the number of tests.

Our contribution. While the qualitative modelling and control concepts of the aforementioned works are aligned with the epidemiological literature, we remark that most of these papers use parameter values collected from previous works or estimated using either different models or from clinical knowledge. Hence, they can't be directly applied to populations with different spatio-temporal patterns. In contrast, the main goal of this paper is to propose a framework which calibrates the model using real-time mobility data from a specific population, measured by Google Mobility through Android devices, and computes an optimal lockdown strategy for that population at any point of the pandemic. To achieve this, we combine parameter estimation for an epidemiological model with a subsequent optimal control step. Secondly, our framework includes the computation of the optimal lockdown policy in a nonlinear model predictive control framework, leading to a robust feedback protocol which allows real-time adaptation of the release strategy.

Methodological summary. Our epidemiological model simulates the transmission dynamics of COVID-19 spread in the English population (see Section 2) using the anonymised data on the reduction of the population mobility collected through smartphones and released by Google. In Section 3, we further calibrate this model using the data released from Public Health England (PHE) and the National Health Service (NHS) reporting on daily deaths and the number of people in hospitals with COVID-19, using Approximate Bayesian Computation (ABC). In this inferential framework, we assume that we start with a prior distribution for each parameter value and given a dataset with an inherent observation noise, we obtain a non-parametric estimate of a probability distribution for each of the parameter values. This allows us to estimate parameters of our model for the specific case of England, as opposed to inheriting parameters from epidemiological models from other countries. Some key attributes of our model are the inclusion of age-dependent transition probabilities between the different compartments which are also estimated from data, as well as age-dependent social distancing, and the use of Google mobility data to quantify the effect of social distancing measures in reality. Having calibrated our model, in Section 4 we design a lockdown strategy which is differentiated according to social contact categories including schools, work, and others. This allows us to assign a different economic penalty for each one of them. Borrowing a leaf from optimal control theory, we synthesize an optimised lockdown and exit strategy which minimizes the number of COVID-19-related casualties in the population, but also taking into account economic constraints. In order to perform this task, we quantify the relation between the decrease in social contacts with the reduction in the population mobility and optimise with respect to the latter, which is an effectively measurable quantity compared to an abstract decrease in social contacts.

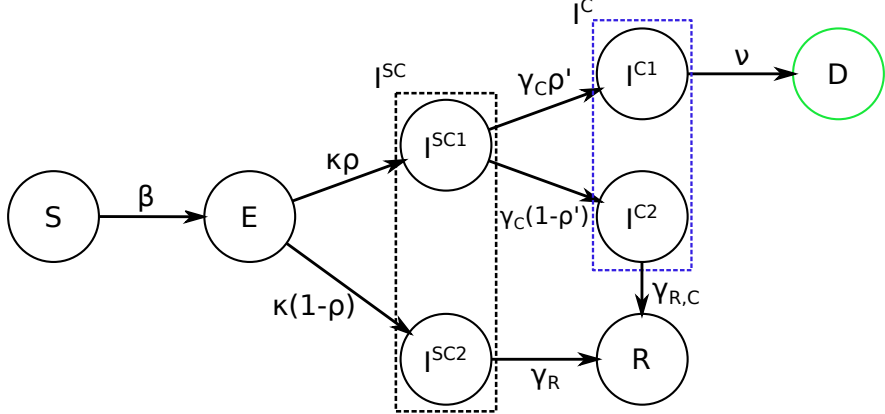


Figure 1: Graphical representation of the model, for each age group. The green color represents a compartment that is observed independently for each age group, while blue represents a compartment whose sum across age groups is observed.

2 Using Google mobility to model epidemics

Our epidemiological model is developed in order to exploit data on change of mobility (in our case, provided by Google) and information on the social contacts patterns at different types of locations in the UK, such as schools or workplaces, estimated by the BBC Pandemic project [Klepac et al., 2020] and the POLYMOD study [Prem et al., 2017]. Presently, our analysis focuses only on England; we stress, however, that the methodology can be extended to consider the whole of the UK or any other country, where suitable data is available. In this Section, we first explain the fundamental dynamic properties considered in our model and then explain how these two data sources are used in our compartmental model in Subsection 2.1.

Model dynamics Assuming a well-mixed population¹, we consider a compartmental model [Anderson and May, 1992], splitting the population in different *compartments* representing different states of the infection:

- Susceptible (S), meaning people who did not have any contact with the infection,
- Exposed (E) to the infection, but not yet infectious,
- Infected SubClinical (I^{SC} , split in I^{SC1} and I^{SC2}), not needing medical attention,
- Infected Clinical (I^C , split in I^{C1} and I^{C2}), needing medical attention,
- Recovered (R), which we assume are resistant to a new infection,
- Deceased (D).

As strong evidence towards the age-dependent severity of COVID-19 has been observed in previous research works [Hilton and Keeling, 2020, Davies et al., 2020], we consider age-stratification of all of the states along 5 age groups: 0-19, 20-39, 40-59, 60-79, 80+, hence we will use the notation E_i to denote the exposed population in the i -th age group, and similarly for the other states. The model will assume that all the age groups are susceptible to the infection in the same way, but that the severity is strongly dependent on the age of the patient through the age-dependent probabilities of necessity of hospitalization (ρ_i) and death if hospitalized (ρ'_i) for the i -th age group.

Another key assumption of our model is that when a patient is hospitalized and diagnosed, they are isolated and therefore not able to spread the infection. To reflect this scenario, we assume that from the exposed state and after some incubation period, all patients will become sub-clinical I^{SC} , in which state they

¹Namely, each person has the same probability of interacting with any other person in the population. Although this is extremely simplifying, compartmental models under this assumption are widely used to describe the dynamics of epidemics over large populations.

are infectious. Afterwards, some of them will recover (R) and others will need clinical help (I^C); we model this by splitting I^{SC} into two categories: the ones recovering straightaway (I^{SC2}) and the ones in need of clinical care (I^{SC1}). The split happens with an age-dependent probability ρ_i . After some time, people in I^{SC1} will go to hospital, therefore moving to the I^C state; similarly as before, the latter state is split in two categories according to the final outcome: the ones in I^{C1} will decease (D) after some time, while the ones in I^{SC2} will recover (R). This split is again described by an age-dependent probability, which we denote as ρ'_i . A visualization of the dynamics is given in Figure 1. Mathematically, this can be described using the following system of ODEs:

$$\frac{dS_i}{dt} = -\beta S_i \sum_j C_{ij} \frac{I_j^{SC}}{N_j} \quad (1)$$

$$\frac{dE_i}{dt} = \beta S_i \sum_j C_{ij} \frac{I_j^{SC}}{N_j} - \kappa E_i \quad (2)$$

$$\frac{dI_i^{SC1}}{dt} = \rho_i \kappa E_i - \gamma_C I_i^{SC1} \quad (3)$$

$$\frac{dI_i^{SC2}}{dt} = (1 - \rho_i) \kappa E_i - \gamma_R I_i^{SC2} \quad (4)$$

$$\frac{dI_i^{C1}}{dt} = \rho'_i \gamma_C I_i^{SC1} - \nu I_i^{C1} \quad (5)$$

$$\frac{dI_i^{C2}}{dt} = (1 - \rho'_i) \gamma_C I_i^{SC1} - \gamma_{R,C} I_i^{C2} \quad (6)$$

$$\frac{dR_i}{dt} = \gamma_{R,C} I_i^{C2} + \gamma_R I_i^{SC2} \quad (7)$$

$$\frac{dD_i}{dt} = \nu I_i^{C1}, \quad (8)$$

where $I_j^{SC} = I_j^{SC1} + I_j^{SC2}$ and C is the contact matrix representing the frequency of contacts between different age groups [Klepac et al., 2020], where each element C_{ij} represents the average daily number of contacts a person in age group i has with people in age group j . To simulate from the model, the ODEs (Equations (1)-(8)) are integrated using a 4th-order Runge Kutta integrator, with a timestep $dt = 0.1$ days; the dynamics is started on the 1st of March.

2.1 Influence of mobility on dynamics

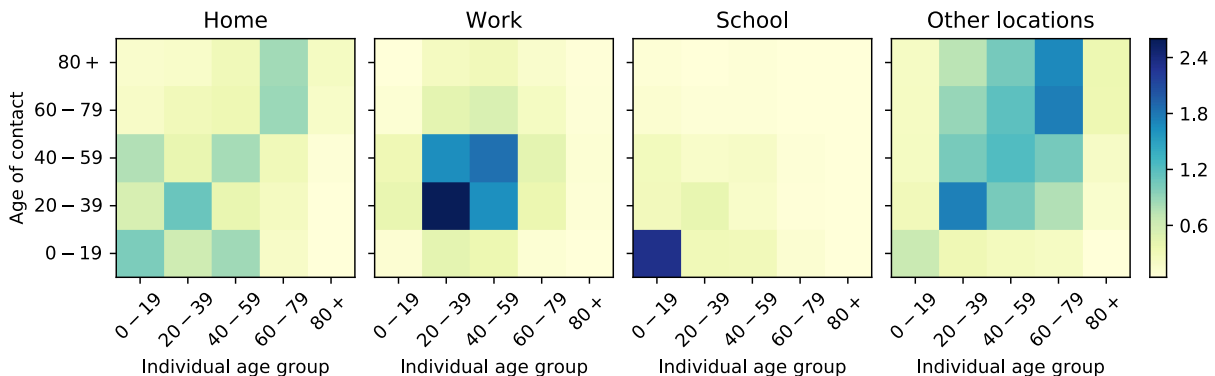


Figure 2: Contact matrices at different locations for the age groups used in the present study (0-19, 20-39, 40-59, 60-79, 80+); these are obtained by aggregating and combining the contact matrices for 5-year bands provided by Klepac et al. [2020] and Prem et al. [2017].

The contact matrices are a crucial component defining our model dynamics. The recent BBC Pandemic project [Klepac et al., 2020] estimated such matrices for the specific case of the UK; however, for legal reasons, this study did not involve any participants younger than 12 years old. We therefore exploit the previous POLYMOD study [Prem et al., 2017] to integrate this missing information; to do this, we follow the procedure described in Klepac et al. [2020].

The BBC Pandemic project also contains information according to the contact being physical or conversational and on weekdays/weekends, which we aggregate combining these classifications. Finally, the age groups considered in these studies (namely, 5 year bands) are finer than the ones we consider in the present work; we therefore aggregate the data to make contact matrices to suit our needs. The (i, j) -th entry of this contact matrices at different locations (eg. home, workplace, school and other locations) represent the amount of daily contacts an individual in age group i has with individuals from age group j in different settings (see Figure 2). Before the lockdown, the total contact matrix is simply the sum of the contributions of these different locations:

$$C = C^{home} + C^{work} + C^{school} + C^{other}.$$

However, the introduction of lockdown measures lead to considerable change to people's social activity and mobility; we model this by introducing a set of multipliers (for each age group and for each of the locations) which will represent the change in the number of social contacts:

$$C_{i,j} = \alpha_i^{home} C_{i,j}^{home} + \alpha_i^{work} C_{i,j}^{work} + \alpha_i^{school} C_{i,j}^{school} + \alpha_i^{other} C_{i,j}^{other}, \quad (9)$$

where α_i^* , for $\star \in \{school, other, work\}$, represents the change of social contacts for age group i in category \star . These multipliers are a function of time and not easily accessible. Instead, it is rather easy to measure the reduction of people's mobility towards the different locations; we choose then to express the α 's as a function of the mobility values provided by Google, as explained in the next paragraph.

Mobility data was collected by Google to reflect the reduction of the population mobility during lockdown in the UK, by following the movements of Android phones; anonymised data is publicly available ². Even though the data is related to the whole British population, we consider it to be broadly representative of English population too and use it in our model. This dataset captures mobility towards the following locations: "residential", "workplaces", "parks", "retail and recreations", "transit stations" and "grocery and pharmacy", which we denote respectively as $m^{residential}$, m^{work} , m^{parks} , m^{retail} , $m^{transit}$, $m^{grocery}$; the changes in mobility are reported with respect to the baseline values prior to introduction of lockdown measures. As can be seen in left panel of Figure 3, a strong weekly periodicity is present in this data; we therefore use a Savitzky–Golay filter [Savitzky and Golay, 1964] to remove it.

We moreover combined the mobility values m^{parks} , m^{retail} , $m^{transit}$, $m^{grocery}$ in order to obtain an aggregated value for the reduction of mobility towards "other locations": $m^{other} = 0.1 \cdot m^{parks} + 0.3 \cdot m^{retail} + 0.3 \cdot m^{transit} + 0.3 \cdot m^{grocery}$. Even though the numerical values of the weights are arbitrary, this choice is motivated by our observation that the value of the different contributions of the mobility data is quite similar; we also attribute a smaller value to "parks" as people get less in strict contact with each other there with respect to "retail", "transit" or "grocery" locations.

As no data with regards to schools were provided, we fixed the value of m^{school} to be 0.1 from the 23rd of March on, which is the day since when schools and universities were closed, except for children of essential workers³. The mobility data obtained after the aggregation and smoothing operations described above are presented in the right panel of Figure 3.

In order to connect the reduction in mobility to the reduction in the number of contacts, we proceed in the following way: first we assume that the number of residential contacts stays constant; in fact, we expect the behavior of people at home not to differ too much with respect to what it was prior the introduction of lockdown measures; for our model, this amounts to fixing $\alpha_i^{home}(t) = 1, \forall t, \forall i$. With regards to the remaining contributions to the total number of contacts, we expect data on mobility reduction to be representative of the subset of the population which mostly uses smartphones, which is likely to be younger than 60 years old. Moreover, a large part of the population older than 60 years old does not take part in work or school

²<https://www.google.com/covid19/mobility/>

³See for instance here: <https://www.theguardian.com/world/2020/mar/18/coronavirus-uk-schools-to-be-closed-indefinitely-and-exams-cancelled>.

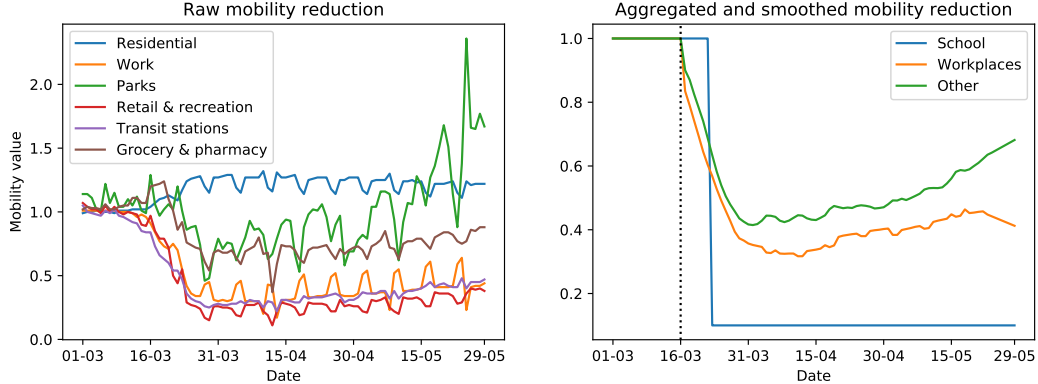


Figure 3: Raw and elaborated mobility data. In the raw mobility data, which is scaled with respect to a baseline value representing average mobility in the months prior to the pandemics, a strong weekly seasonality is present, which we mostly removed by using a Savitzky–Golay filter. Moreover, note that the mobility towards “residential” (which is not used in our analysis) locations is larger during the lockdown months than before, as people spend more time in their homes. Finally, note the very large increase in people’s mobility towards parks due to the end of the winter season. That contribution is however only one of the components in our aggregated m^{other} mobility value, so the latter does not increase that abruptly.

activities. Motivated by these arguments, we define the values of α_i^{school} , α_i^{other} and α_i^{work} separately for population below and above 60. Specifically, we assume the following for age groups below 60 years old (age group index 1,2,3):

$$\alpha_i^{school}(t) = \alpha_{123} \cdot m^{school}(t), \quad \alpha_i^{other}(t) = \alpha_{123} \cdot m^{other}(t), \quad \alpha_i^{work}(t) = \alpha_{123} \cdot m^{work}(t), \quad \text{for } i \in \{1, 2, 3\} \quad (10)$$

where we made the dependence on time explicit in order to highlight that $\alpha_{123} \in [0, 1]$ is a time-independent scalar, which is an additional parameter to our model; this amounts to assuming that the reduction in the number of contacts is due to a combination of reduced mobility and increased awareness of people, for instance by maintaining social distancing. For people above 60 years old (age group index 4 and 5) we assume instead that the reduction in contacts stays constant since the introduction of lockdown measures and that such reduction is equally distributed across to the different categories (as the contacts for *work* and *school* will be relatively few):

$$\alpha_4^{school}(t) = \alpha_4^{other}(t) = \alpha_4^{work}(t) = \alpha_4, \quad \alpha_5^{school}(t) = \alpha_5^{other}(t) = \alpha_5^{work}(t) = \alpha_5, \quad (11)$$

where $\alpha_4, \alpha_5 \in [0, 1]$ are time-independent scalars, which are parameters in our model as well. This latter assumption is motivated by the fact that such part of the population is more susceptible to the disease, so that the official advice will be for them to be as isolated as possible throughout the epidemics.

We initialise our implementation of the model dynamics on the 1st of March and we fix the contact matrix to be the standard one relative to the UK until the introduction of lockdown measures (which we assume to be on the 18th March, i.e. two days after the government advice which asked people to self-isolate⁴); from that day onward, we use the contact matrix obtained from Eq. (9), by fixing $\alpha^{home} = 1$ and obtaining the values for the other α ’s by Eqs. (10) and (11).

2.2 Initialization and model parameters

At the beginning of the dynamics, most of the population is in the *S* state, except for a small number of individuals which seed the infection. We therefore assume that some people were already infected on the 1st of March and we denote that number as N^{in} ; this number is split across the different categories and age groups in the following way:

⁴See for instance description of measures undertaken by the UK government here: <https://bfpg.co.uk/2020/04/covid-19-timeline/>.

- First, the total number of infected population is spread across the age groups with the following rates (from youngest to oldest): 0.1, 0.4, 0.35, 0.1, 0.05; these values come from the assumption that the disease was brought to the UK from abroad through air travel, and approximate the age distribution of flight passengers to the UK⁵.
- Then the number of infected individuals in each age group is split in the E , I^{SC1} and I^{SC2} compartments in the following way:

$$E_i^{in} = N_i^{in}/3, \quad I_i^{SC1,in} = \rho_i N_i^{in} \cdot 2/3, \quad I_i^{SC2,in} = (1 - \rho_i) N_i^{in} \cdot 2/3. \quad (12)$$

The other compartments are initialized to 0, except for S , which is initialized to the total population in the corresponding age group obtained by the 2018 census and provided by the office for national statistics⁶, from which the number of people seeding the infection at the start of the dynamics is subtracted.

Parameters which define the dynamics of our model and need to be calibrated are the following:

- β : probability of a contact between an S and I^{SC} individual resulting in the S individual catching the infection.
- $\kappa = 1/d_L$: transition rate of an Exposed individual becoming Infected SubClinical, with d_L the average number of days in the E state.
- $\gamma_C = 1/d_C$ transition rate of going from I^{SC1} to I^C , with d_C the average number of days it takes to undergo this transition.
- $\gamma_R = 1/d_R$ recovery rate from I^{SC2} , with d_R the average number of days it takes to recover.
- $\gamma_{R,C} = 1/d_{R,C}$ recovery rate from I^C , with $d_{R,C}$ the average number of days it takes to recover.
- $\nu = 1/d_D$ death rate from I^C , with d_D the average number of days before death occurs after entering the I^C state.
- ρ_i 's: age dependent probabilities of going to I^C instead of directly recovering from the I^{SC} state.
- ρ'_i 's: age dependent probabilities of death after being hospitalized.
- N^{in} : total number of individuals who carried the infection at the start of the training period (1st of March).
- α_4 : constant value of reduction in social contacts for people in age group 4, after the beginning of the lockdown period.
- α_5 : constant value of reduction in social contacts for people in age group 5, after the beginning of the lockdown period.
- α_{123} : coefficient of proportionality between reduction of social contacts and reduction of mobility for age groups 1,2,3, as described in Section 2.1.

2.3 The reproduction number \mathcal{R}

We explain here how to compute the reproduction rate (\mathcal{R}) for our model, which is considered as one of the main measures to quantify the spread of an epidemic and the efficiency of our lockdown strategies proposed in Section 4, and measures the average number of secondary infections an infected individual is capable of generating in a fully susceptible population. Our computation strategy follows Gatto et al. [2020]; first, we define the *next generation matrix*, which relates the numbers of newly infected individuals in the various categories in consecutive moments, before and after a contact (in our case, a time step) in the case where one

⁵Check for instance <https://www.statista.com/statistics/304641/age-distribution-of-air-passengers-by-airport-uk/>

⁶<https://www.ons.gov.uk/peoplepopulationandcommunity/populationandmigration/populationestimates/datasets/populationestimatesforukenglandandwalesscotlandandnorthernireland>

single person interacts with a fully susceptible population. To do this, fix $S_i = N_i$ and consider the Jacobian matrix of the infection subsystem – which is composed by states $\{E_i, I_i^{SC_1}, I_i^{SC_2}, I_i^{C_1}, I_i^{C_2}\}$, $i = 1, \dots, 5$ (we note that the states R_i and D_i were removed, as they are “final” states: once an individual is in one of these states, they remain there). Using the same notation as in Gatto et al. [2020], this Jacobian has the following form

$$\mathbf{J}_0 = \begin{bmatrix} -\kappa I & \beta \frac{SC}{N} & \beta \frac{SC}{N} & 0 & 0 \\ \rho \kappa I & -\gamma_C I & 0 & 0 & 0 \\ (1-\rho)\kappa I & 0 & -\gamma_R I & 0 & 0 \\ 0 & \rho' \gamma_C I & 0 & -\nu I & 0 \\ 0 & (1-\rho')\gamma_C I & 0 & 0 & -\gamma_{R,C} I \end{bmatrix},$$

where we note that I is the 5×5 identity matrix, and each zero corresponds to a 5×5 zero matrix. We also slightly abused the notation in the other entries. For example, the matrices $\frac{SC}{N}$, $\rho \kappa I$, etc., are 5×5 matrices whose entries are given by

$$\left(\frac{SC}{N}\right)_{ij} = \frac{S_i C_{ij}}{N_j}, \quad (\rho \kappa I)_{ij} = \kappa \rho_i \delta_{ij},$$

where δ_{ij} is the Kronecker delta, and similarly for the other matrices.

The matrix \mathbf{J}_0 is decomposed into the *transmission matrix*, T , and the *transition matrix*, Σ , defined as follows:

$$T = \begin{bmatrix} 0 & \beta \frac{SC}{N} & \beta \frac{SC}{N} & 0 & 0 \\ 0 & 0 & 0 & 0 & 0 \\ 0 & 0 & 0 & 0 & 0 \\ 0 & 0 & 0 & 0 & 0 \\ 0 & 0 & 0 & 0 & 0 \end{bmatrix}, \quad \Sigma = \begin{bmatrix} -\kappa I & 0 & 0 & 0 & 0 \\ \rho \kappa I & -\gamma_C I & 0 & 0 & 0 \\ (1-\rho)\kappa I & 0 & -\gamma_R I & 0 & 0 \\ 0 & \rho' \gamma_C I & 0 & -\nu I & 0 \\ 0 & (1-\rho')\gamma_C I & 0 & 0 & -\gamma_{R,C} I \end{bmatrix} = \mathbf{J}_0 - T.$$

The *next generation matrix* is then defined as $K_L = -T\Sigma^{-1}$. The reproduction number \mathcal{R} is the *spectral radius* of this matrix, namely the absolute value of its largest eigenvalue, which represents the secondary number of infections a single infected individual is capable of generating in a fully susceptible population. As T depends on the contact matrix C , the reproduction number will be a function of the Google mobility for different locations ($m^{school}(t)$, $m^{work}(t)$ and $m^{other}(t)$). Hence, we will focus on studying the evolution of $\mathcal{R}(t)$ over time.

3 Model calibration

We use approximate Bayesian computation (ABC) [Lintusaari et al., 2017] to calibrate the parameters of the model described in Subsection 2.2, by using the following datasets reporting on the number of hospitalized and deceased patients with positive tests for COVID-19 in England and which are released by the NHS and PHE:

- The daily number of deaths in hospitals attributed to COVID-19 (per age group) is released by NHS England⁷. The data starts from the 1st of March, with one death reported before that date, which we drop from our analysis.
- The daily number of hospitalized people with COVID-19 related diseases is obtained from the supporting material of the government daily press conference⁸. Data is available from the 18th of March.

We calibrate our model on data from the 1st of March up to different ending times T_{obs} (11th of April, 26th of April, 11th of May and 23rd of May), in order to study the change in parameter values with different data sizes.

Moreover, ABC allows us to fix a prior range for the parameters and uncertainty on them (defined by a prior distribution $\pi(\theta)$), and to obtain an uncertainty range in the prediction, which we will use in designing

Parameter	β	d_L	d_C	d_R	$d_{R,C}$	d_D	N^{in}	α_{123}	α_4	α_5
Prior lower bound	0	1	1	1	4	1	0	0.3	0	0
Prior upper bound	0.5	10	10	10	14	10	500	1	1	1
Parameter	ρ_1	ρ_2	ρ_3	ρ_4	ρ_5	ρ'_1	ρ'_2	ρ'_3	ρ'_4	ρ'_5
Prior lower bound	0	0	0	0	0.5	0	0	0	0	0.5
Prior upper bound	0.3	0.5	1	1	1	1	1	1	1	1

Table 1: Bounds for uniform priors for the model parameters.

the optimal control task (Section 4). In contrast with existing works, we perform joint parameter inference on 20 parameters; for all of them, we choose a uniform prior, whose ranges are given in Table 1.

3.1 Approximate Bayesian Computation

Approximate Bayesian computation (ABC) gives an approximation of the posterior distribution of the parameters, starting from a prior $\pi(\theta)$ and a (possible stochastic) simulator model $M(\theta)$, for which the likelihood $p(\mathbf{x}|\theta)$ cannot be computed. Specifically, the true posterior is obtained via Bayes' theorem as

$$\pi(\theta|\mathbf{x}^{obs}) = \frac{\pi(\theta)p(\mathbf{x}^{obs}|\theta)}{p(\mathbf{x}^{obs})}.$$

In ABC, we approximate this expression by looking for the values of the parameters which best approximate the observations. The fundamental ABC rejection sampling scheme iterates the following steps:

- Draw θ from the prior $\pi(\theta)$.
- Simulate a synthetic dataset \mathbf{x}^{sim} from the simulator-based model $M(\theta)$.
- Accept the parameter value θ if $\mathbf{d}(\mathbf{x}^{sim}, \mathbf{x}^{obs}) < \gamma$. Otherwise, reject θ .

Here, the metric on the dataspace $\mathbf{d}(\mathbf{x}^{sim}, \mathbf{x}^{obs})$ measures the closeness between \mathbf{x}^{sim} and \mathbf{x}^{obs} . The accepted values of θ are thus sampled from a distribution $\pi_{ABC}(\theta|\mathbf{x}^{obs}) \propto \pi(\theta)p_{\mathbf{d},\gamma}(\mathbf{x}^{obs}|\theta)$, where $p_{\mathbf{d},\gamma}(\mathbf{x}^{obs}|\theta)$ is an approximation to the intractable likelihood function $p(\mathbf{x}^{obs}|\theta)$:

$$p_{\mathbf{d},\gamma}(\mathbf{x}^{obs}|\theta) = \int p(\mathbf{x}^{sim}|\theta) \mathbb{K}_\gamma(\mathbf{d}(\mathbf{x}^{sim}, \mathbf{x}^{obs})) d\mathbf{x}^{sim}.$$

Here, $\mathbb{K}_\gamma(\mathbf{d}(\mathbf{x}^{sim}, \mathbf{x}^{obs}))$ is a probability density function proportional to $\mathbf{1}\{\mathbf{d}(\mathbf{x}^{sim}, \mathbf{x}^{obs}) \leq \gamma\}$, $\mathbf{1}\{\cdot\}$ being an indicator function which equals 1 when the condition in the brackets is true and 0 otherwise.

This guarantees that, in principle, the above approximate likelihood converges to the true one when $\gamma \rightarrow 0$. In this paper, we used the PMCAABC algorithm [Beaumont, 2010] as implemented in the Python library ABCpy [Dutta et al., 2017] allowing efficient parallelization using MPI, to perform parameter inference. This is an iterative algorithm considering a set of points $\{\theta_i\}$ which are given a certain weight representing how much the sample x_i generated by each of them is close to the observation. The algorithm proceeds by iteratively perturbing the parameters and performing simulations from the model, and reducing the threshold γ so that the approximation to the posterior distribution improves. At the end of the algorithm, a weighted set of parameter points which are samples from the approximate posterior $\pi_{ABC}(\theta|\mathbf{x}^{obs})$ is returned.

For the sake of calibrating the model, we want to match the number of people in I^C (summed over all age groups) and the daily deaths, by date of reporting, for each of the 5 considered age groups; the model is structured so that it returns those values as outputs. Therefore, we consider the set of variables $\mathbf{x} = ((\Delta D_1(t), \Delta D_2(t), \Delta D_3(t), \Delta D_4(t), \Delta D_5(t))_{t=1}^T, (I_{tot}^C(t))_{t=1}^T)$ where we denote by t the day since the

⁷<https://www.england.nhs.uk/statistics/statistical-work-areas/covid-19-daily-deaths/>

⁸<https://www.gov.uk/government/publications/slides-and-datasets-to-accompany-coronavirus-press-conference-25-may-2020>

start of the dynamics, by $\Delta D_i(t) = D_i(t) - D_i(t-1)$ the deaths occurring on day t in age group i , and we consider $I_{tot}^C(t) = \sum_{i=1}^5 I_i^C$. The corresponding observation is denoted as:

$$\mathbf{x}^{obs} = ((\Delta D_1^{obs}(t), \Delta D_2^{obs}(t), \Delta D_3^{obs}(t), \Delta D_4^{obs}(t), \Delta D_5^{obs}(t))_{t=1}^T, (I_{tot}^{C,obs}(t))_{t=1}^T).$$

As discussed in Section 2, data on I^C is available only from the 18th of March, and therefore we discarded the first 17 days for the corresponding observations.

We now define a distance for ABC that enables us to make use of the above data, by relying on a weighted sum of the pointwise Euclidean distances between the different elements of the trajectories. Specifically, let us denote the pointwise Euclidean distances between the different elements of simulated and observed data by:

$$d_{D,i} = \sum_{t=1}^T (\Delta D_i(t) - \Delta D_i^{obs}(t))^2, \quad d_I = \sum_{t=18}^T (I_{tot}^C(t) - I_{tot}^{C,obs}(t))^2.$$

Using this, the final distance we consider is:

$$d(\mathbf{x}, \mathbf{x}^{obs}) = \sum_{i=1}^5 d_{D,i} w_{D,i} + w_I d_I,$$

where $w_{D,i}$ and w_I are weights which we can fix according to considerations on the speed of convergence. It is clear that the above, being a combination of Euclidean distances, is a valid distance for \mathbf{x} for each choice of the weight; the latter however are important for the ABC algorithm in practice, as they force the algorithm to constrain more or less on some of the distances. The weights we have found to work best for the problem at hand (as they gave faster convergence) are: $w_D = (1, 1, 1, 2, 2)$ and $w_I = 0.1$.

3.2 Inferred parameters

We calibrate our model on data up to four different days representing different stages of the epidemic (11th of April on the peak of the epidemic and further towards the tail, up to the 23rd of May, as shown in Figure 4). The availability of the amount of data over those four days affects how well our model was able to

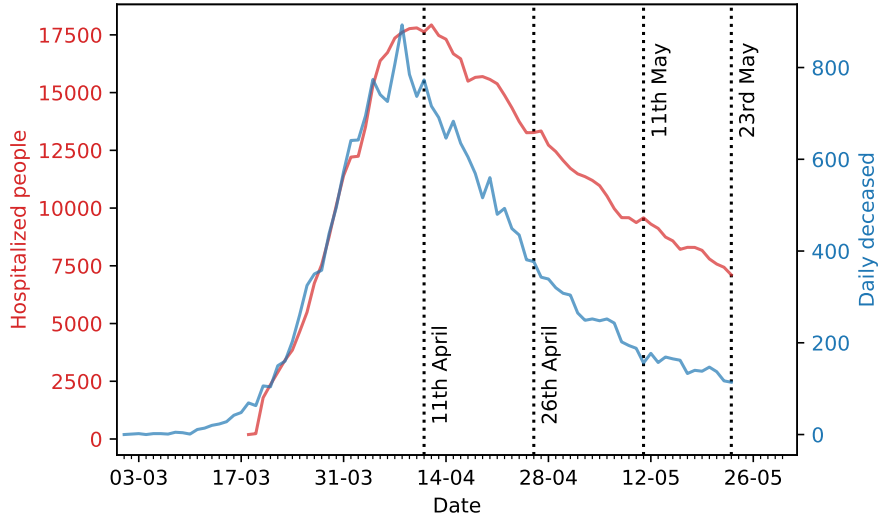


Figure 4: Evolution of the epidemics in England, together with ending dates of the observation period T_{obs} used in this study. The red line represents the number of hospitalized people (scale on y axis on the left), while the blue line represents the daily number of deaths (scale on right).

fit the data and predict the future. We have drawn independent and identically distributed (i.i.d) samples⁹ from the approximate posterior distribution $\pi_{ABC}(\theta|\mathbf{x}^{obs})$ of the parameters in all of these scenarios. We report the posterior mean and the corresponding standard deviation for each model parameter and for each observation horizon T_{obs} in Table. 2. We notice that the estimated values differ slightly over the days, but they are quite similar on 11th and 23rd of May as in those days we do not observe any significant changes in the dynamics of the epidemics. In Figure 5, we report the estimated marginal posterior distributions of the age-dependent probabilities of hospitalization and dying once hospitalized inferred using data until the 23rd of May; in these figures, we use violin plots to represent the marginal distribution of each parameter value. As point estimates and marginal posterior distributions may not be able to capture the correlations present between parameters, we report the inferred joint posterior distributions between pairs of these parameters in Appendix B to provide a complete picture.

Observation period	d_L	d_C	d_R	$d_{R,C}$	d_D
1st March-11th Apr	3.09 ± 1.78	4.12 ± 2.16	2.90 ± 1.92	9.94 ± 2.67	4.98 ± 2.35
1st March-26th Apr	1.61 ± 0.51	2.46 ± 1.12	1.67 ± 0.50	11.42 ± 1.83	5.19 ± 2.33
1st March-11th of May	1.50 ± 0.43	2.24 ± 0.87	1.81 ± 0.68	11.95 ± 1.60	5.83 ± 2.14
1st March-23rd of May	1.57 ± 0.42	2.12 ± 0.80	1.54 ± 0.40	12.08 ± 1.51	5.54 ± 2.19
Observation period	β	α_{123}	α_4	α_5	N^{in}
1st March-11th Apr	0.13 ± 0.06	0.48 ± 0.15	0.39 ± 0.26	0.68 ± 0.23	303 ± 132
1st March-26th Apr	0.13 ± 0.03	0.64 ± 0.18	0.50 ± 0.25	0.74 ± 0.19	249 ± 140
1st March-11th of May	0.12 ± 0.03	0.59 ± 0.19	0.54 ± 0.27	0.75 ± 0.20	264 ± 131
1st March-23rd of May	0.13 ± 0.03	0.63 ± 0.21	0.57 ± 0.23	0.71 ± 0.23	276 ± 133
Observation period	ρ_1	ρ_2	ρ_3	ρ_4	ρ_5
1st March-11th Apr	0.08 ± 0.07	0.11 ± 0.12	0.16 ± 0.16	0.52 ± 0.25	0.81 ± 0.14
1st March-26th Apr	0.08 ± 0.07	0.10 ± 0.12	0.10 ± 0.08	0.51 ± 0.21	0.82 ± 0.13
1st March-11th of May	0.07 ± 0.07	0.04 ± 0.04	0.09 ± 0.08	0.59 ± 0.23	0.83 ± 0.13
1st March-23rd of May	0.06 ± 0.06	0.05 ± 0.05	0.08 ± 0.08	0.54 ± 0.22	0.79 ± 0.14
Observation period	ρ'_1	ρ'_2	ρ'_3	ρ'_4	ρ'_5
1st March-11th Apr	0.28 ± 0.26	0.21 ± 0.23	0.26 ± 0.26	0.42 ± 0.22	0.82 ± 0.12
1st March-26th Apr	0.28 ± 0.23	0.22 ± 0.23	0.33 ± 0.26	0.35 ± 0.16	0.80 ± 0.13
1st March-11th of May	0.29 ± 0.26	0.35 ± 0.32	0.31 ± 0.24	0.29 ± 0.14	0.78 ± 0.14
1st March-23rd of May	0.26 ± 0.23	0.28 ± 0.25	0.33 ± 0.27	0.26 ± 0.11	0.80 ± 0.13

Table 2: Estimated posterior mean and standard deviation of model parameters, using the different horizons for fitting the model. We note the large standard deviation for the ρ and ρ' parameters related to younger age groups, with respect to the older age groups. This is due to the fact that less information is available with regards to the severity of infection for those age groups, thus rendering the estimate harder. This also proves the ability of our technique to assign meaningful uncertainty ranges. we also point out that the estimated standard deviation is larger than the posterior mean for some of the parameters; this is due to the fact that the posterior distribution is not centered on the posterior mean but skewed; see Appendix B for more details on the shape of the posterior distributions.

As devising a successful lockdown strategy depends on the accuracy of the prediction of our model, we compare the predicted number (median prediction and 99 percentile credibility interval) of hospitalized people and daily deaths of our calibrated model with real data on these four observation horizons. To do this, we integrate the dynamical model using posterior samples from the ABC posterior distribution on each of these days and we show our results in Figure 6. Additionally, we provide the estimated basic reproduction number \mathcal{R} from the dynamics obtained from the posterior sample points, and plot that with the relative credibility bands. We note that, with the exception of the model calibrated on data until the 11th of April, the estimated reproduction number has a value larger than 2 before the introduction of containment measures by the government, which then decreases below 1 a few days afterwards, and remaining below one until the

⁹Note that the ABC inference scheme provides us with a set of samples from the posterior distribution associated with the importance weights. Then, in order to get i.i.d. samples from it, we *bootstrap* them, namely we choose (with replacement) from the set of ABC samples with probability proportional to the importance weight itself.

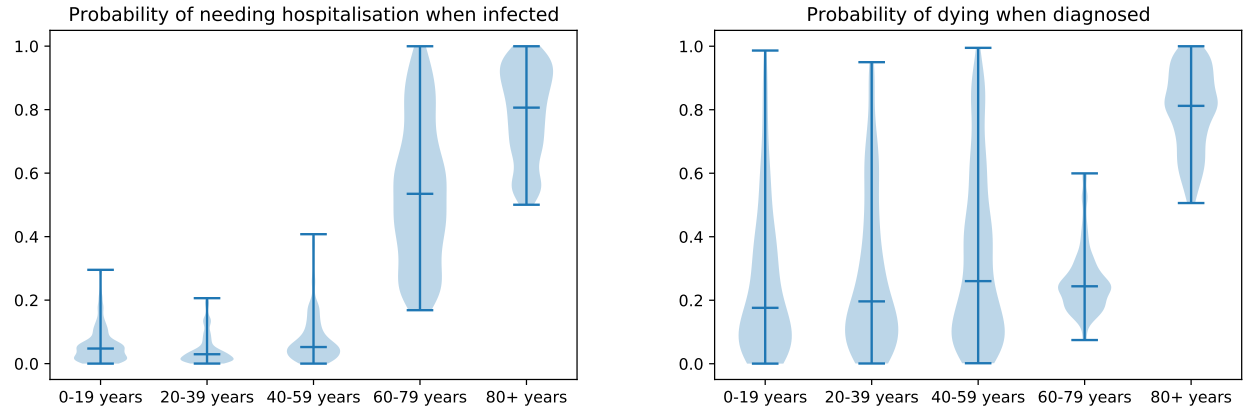


Figure 5: Violin plots representing the inferred marginal posteriors for age-dependent probabilities, using data until the 23rd of May. In the right panel, note the larger uncertainty for the ρ' values corresponding to younger age groups, due to relatively little deaths amongst people younger than 60, with respect to people above that age. For the same reason, in the left panel the probability of being hospitalized for people younger than 60 is estimated to be between 0 and 0.2 with large confidence.

end of the training period. We also note that towards the end of the training period, the credibility interval includes some values above 1, due to the fact that the values of people’s mobility have increased in later weeks. Finally, plots comparing the daily number of deaths with real data stratified by age groups together with additional results on the evolution of the other compartments are reported in Appendix A.

The results presented in Figure 6 highlight that it is hard to forecast precisely the evolution of the epidemic with a simple compartmental model as the one we consider. This can be seen from the fact that using different observation horizons to determine the parameters of the model leads to very different predictions of the evolution; this phenomenon is extremely evident in the first line of Figure 6 (i.e. using data until the 11th of April), where the predicted number of deaths and hospitalized people is much larger than what eventually turned out to be the case (we remark that the prediction is taking into account the measured mobility even throughout the prediction horizon). We also remark that our model systematically overestimates the number of deceased in the tail of the epidemics; this could probably be explained by the fact that it does not take into account the increased capacity of the health system to fight the disease.

4 Computing optimised mobility values

We now adopt the viewpoint of a policy maker whose task is to determine mobility restrictions on a population in order to slow down the spread of the COVID-19 epidemics, while still keeping the economic costs of lockdown as low as possible. We therefore formulate the problem in an optimal control setting. In this context, we will minimise a cost functional which includes penalties on the number of COVID-19 related deaths, ICU beds occupancy, and the economic cost of different types of lockdown.

The control variables in our problem are the reductions of the mobility values m^{school} , m^{work} , m^{other} defined in Sec. 2 (Mobility data). These are related to the coefficients in the contact matrices α^{school} , α^{work} , α^{other} via the inferred values α_{123} , α_4 and α_5 in (10), relating our control policy to measurable quantities. We remark here that the mobility values m^* , for $\star \in \{school, other, work\}$ only control the change of contacts for age groups 1,2,3 (below 60 years old), while the change of contacts for age groups 4,5 (above 60) is instead represented by the parameters α_4, α_5 , which we inferred from data. Our optimisation framework therefore assumes that the reduction in social contacts for age groups (4,5) stays fixed to the inferred value throughout the optimisation horizon, and we instead optimise only on the change of mobility referred to younger age groups. This is reasonable as the older age groups constitute a minor part of the workforce and are the extremely vulnerable to the disease. Therefore, we expect that the official advice for them will be to remain with stricter isolation rules than the rest of the (working) population.

To obtain the optimal strategy, we need to know the estimated value of the parameters of the model, for

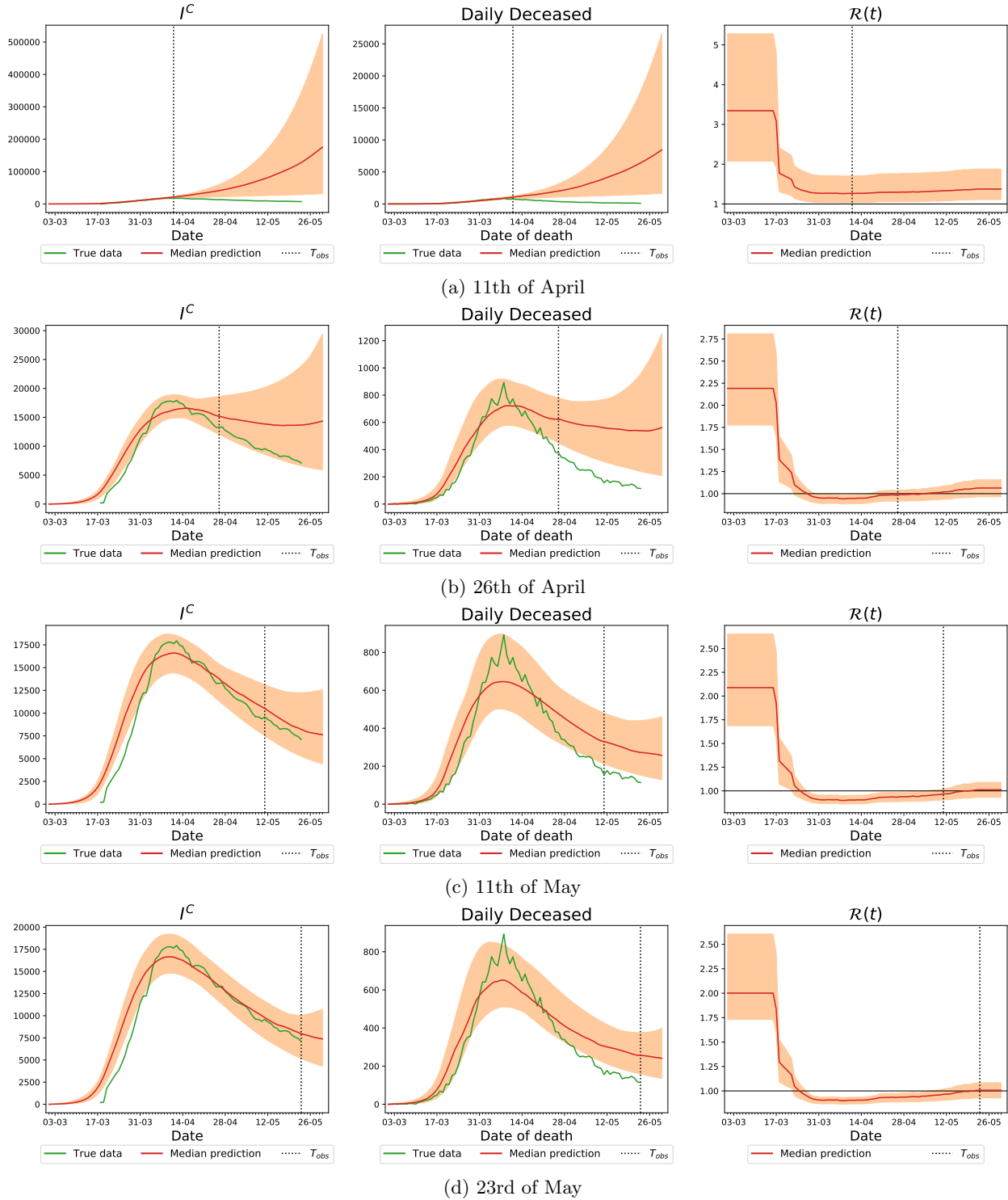


Figure 6: Comparison of predictions of our model with the real number of hospitalized people with COVID-19 and total daily deaths (green). The solid red line denotes the median prediction, filled spaces denote the 99% credible interval and the vertical dashed line denotes the observation horizon. The different rows represent different observation horizons, while the columns represent number of people in hospital (I^C compartment, left column), daily deceased (middle column) and value of $\mathcal{R}(t)$ (right column).

which we could have considered the posterior means provided in Table 2.

However, given that we have the whole information on the posterior distribution, we will pose the control problem using the *integrated posterior*; this encompasses using various sets of values of the parameters sampled from the posterior distribution and running the model forward using these parameters - the cost functional is then evaluated over all these simulations and behaves as an expected value over different possibilities. We remark that, even though this is computationally costly, it pays off by offering a control strategy that is robust to a number of possible (and highly likely) scenarios, by taking into account the uncertainty on parameter estimates [Albi et al., 2020].

In Section 4.1 and 4.2, we devise an optimal lockdown strategy starting on the 24th of May using the posterior distribution of the model parameters inferred using the data available until the 23rd of May. In Section 4.3 we instead show how to dynamically update the optimal control strategy by re-calibrating the model once new data becomes available.

4.1 Cost functional and control strategy

In this section, we define the control problem we aim to solve and describe the optimal control methodology adopted in this paper. Let us denote as t_0 the start of the optimisation interval, corresponding to the day we wish to start the new lockdown policy (in our first example, the 24th of May), and by T_h the length of the interval in days, for which we want to apply the lockdown strategy, also known as optimisation horizon.

We consider a cost functional which combines the economic cost of lockdown with the sanitary cost of lifting restrictions. We point out that the relative weight of these costs allows us to input different political strategies, such as favouring a strict lockdown at a high economic cost, or vice versa. To consider the cost of lifting restrictions, we penalise the predicted number of deaths during the optimisation horizon $[t_0, t_0 + T_h]$. This is given by

$$\sum_i (D_i(t_0 + T_h) - D_i(t_0)) = \sum_{t=t_0+1}^{t_0+T_h} \sum_i \Delta D_i(t),$$

where $\Delta D_i(t)$ is the daily increase in the number of deceased in the age group i . Furthermore, to ensure that the NHS capacity is not surpassed, we would like to guarantee that the number of infected individuals who need hospitalisation, $I^C = \sum_i I_i^{C_1} + I_i^{C_2}$, remains below the NHS capacity. This could be included as a hard state constraint, here instead we penalise the event in which I^C surpasses the NHS limit, NHS_{\max} , by including a term of the form

$$\Phi(I^C) := \max(I^C - NHS_{\max}, 0).$$

We point out that this term is not activated in our current example. The levels of infected people who need hospitalisation at the moment remain well below the NHS threshold – which here we take to be $NHS_{\max} = 10000^{10}$. For example, the number of people in hospital with COVID-19 related symptoms at the end of our training window (23rd of May) was 7106, while at the height of the peak of the epidemic in England (on the 12th of April) this number was 17933. If these values ever return to this peak, the NHS capacity term plays a very important role and needs to be taken into account, and for this reason we include it here as a proof of concept. As a final measure of the sanitary cost, we introduce a final penalisation, where we penalise the \mathcal{R} number at the end of the optimisation horizon $\mathcal{R}(t_0 + T_h)$. This terminal penalty ensures that the control strategy does not simply output an optimal solution which switches off the reduction on mobility towards the end of the optimisation horizon. While such a solution is consistent with the optimal control design and is an interesting instance of the turnpike phenomenon [Trélat and Zuazua, 2015], it is not suitable in our context. Finally, to account for the economic cost of lockdown, we penalise the mobility reduction by introducing a quadratic cost of the form $\|\mathbf{1} - m^*(t)\|^2$, for $\star \in \{\text{school, other, work}\}$.

As mentioned before, the forward model is run for different sets of parameters drawn from the posterior distribution obtained via ABC inference. For this reason, the $\Delta D_i(t)$ and $I_i^C(t)$ variables appearing in the cost functional depend on the chosen value of the parameters of the model. We hide the explicit dependence for notational convenience. The cost is computed by taking an expectation over the posterior distribution for the parameters. Each parameter value will lead to a different realisation of the dynamics. Note that,

¹⁰This is the average number of unoccupied general and critical care beds from January to March 2020 in England, see <https://www.england.nhs.uk/statistics/statistical-work-areas/bed-availability-and-occupancy/bed-data-overnight/>

due to the nonlinearity of the system, this is clearly not the same as minimizing the objective using the posterior mean of the parameters only. In practice, we use 50 i.i.d. samples from the posterior distribution and approximate the expectation with an average over the trajectories obtained with those parameter values. Minimizing an expected cost in this way is much more computationally expensive than a cost computed on a point estimate of the parameters (for instance the posterior mean). However, it provides a way to take into account the uncertainty in the parameters.

Collecting the different terms in our cost, we optimise

$$\min_{m(\cdot) \in \mathcal{M}} \mathcal{J}(m) := \sum_{t=t_0+1}^{t_0+T_h} \left[\frac{1}{2} \mathbb{E} \left[\sum_i \Delta D_i(t) + \phi(I^C(t)) \right] + \sum_{\star \in \{s, o, w\}} \frac{\epsilon_\star}{2} \|\mathbf{1} - m^\star(t)\|^2 \right] + \mathcal{R}(t_0 + T_h), \quad (13)$$

through the control signal

$$m(t) = (m^{school}(t), m^{work}(t), m^{other}(t)) \in \mathcal{M} := \{m : [t_0, t_0 + T_h] \rightarrow [0, 1]^3\},$$

where ϵ_\star , for $\star \in \{school, other, work\}$, represents the relative cost of limiting the mobility to schools, workplaces and other locations with respect to the sanitary cost, and where the expectation is taken over the posterior distribution of the parameters of the model. The choice of the values for ϵ_\star affects the optimal policy by attributing a larger economic or social cost of closing one of the categories with respect to the others. Determining adequate weights for these costs is the ultimate task of the policy maker. Here, we present a methodology for the computation of optimal policies and discuss several possible choices for these relative weights.

To close our optimal control formulation we add specifications to the controls we expect to obtain, restricting the space of admissible signals. As discussed in Section 2, the values of α are between 0 and 1, and therefore we expect the m^\star to be in the interval $[0, 1]$ as well, for $\star \in \{school, work, others\}$. This would be a reasonable assumption. However, due to the fact that we cannot impose a 100% closure of all settings, we set a lower bound for m^\star to be the *lowest value* of each m^\star observed during the lockdown. This results in the constraints $m^{work} \in [0.31, 1]$, $m^{school} \in [0.1, 1]$, and $m^{others} \in [0.41, 1]$.

As can be seen from equation (13), the controls m^\star are time-dependent, and they are computed by minimising the cost functional (13) subject to the state constraints (1)-(8). Ideally, the numerical realization of the optimal control strategy would be driven by the calculation of first-order optimality conditions and a reduced gradient approach to minimise $\mathcal{J}(m)$. However, the nonlinearities in the dynamics and in the terminal penalty, where the reproduction rate is expressed as an eigenvalue of parameter-dependent matrix, make our problem highly non-convex. Moreover, the penalty $\Phi(I^C)$ is non-differentiable. For the purposes of this paper we will compute the optimal control by using generalized simulated annealing (or dual annealing) [Xiang and Gong, 2000] as implemented in the `scipy` [Virtanen et al., 2020] Python library. The use of meta-heuristics for the solution of large-scale nonlinear optimal control problems has been assessed in [Albi et al., 2016, Bailo et al., 2018].

Nonlinear Model Predictive Control We embed the solution of the optimal control problem (13) in a nonlinear model predictive control (NMPC) framework [Grüne and Pannek, 2017]. To this end, we select a prediction horizon T_{opt} , and optimise the control variables $m^\star(t)$, $t \in [t_0, t_0 + T_{opt}]$ using the current state at t_0 as our initial condition. From the optimal control sequence we recover the optimal action for a single day, that is $m^\star(t)$, $t \in [t_0, t_0 + 1]$ and evolve the dynamics for the same amount of time, and repeat the optimisation procedure in the updated time frame $[t_0 + 1, t_0 + 1 + T_{opt}]$. This process is then repeated until the complete optimisation interval $[t_0, t_0 + T_h]$ is covered. The NMPC methodology recovers a robust optimal control law in feedback form that can be adjusted to account for disturbances in the control loop. Therefore, instead of using the current state predicted by the model as initial condition, we can update this to be the current state of the population in England estimated from data, every time new data becomes available. This ensures that the control methodology accounts for noisy observations, or for unexpected variations in the data. We exemplify this control methodology and its robustness to the various aspects described in this section in Figures 7-9. In each of the figures, we plot the number of hospitalised people (red full curve) for each control strategy – these results are associated with the red axis, on the left of the figure – and the value of the mobility m^\star in blue, associated with the blue values on the right. The full, dashed, and dash-dotted

lines correspond to work, school and other settings, respectively. We denote by the vector $(\epsilon_s, \epsilon_w, \epsilon_o)$, the different penalties for schools, work, and other locations, respectively.

A crucial issue in the NMPC framework is the selection of the prediction horizon T_{opt} . For small prediction horizons, the optimal action tends to be instantaneous and loses its capability to foresee long-term consequences of the policy. On the other hand, a sufficiently long prediction horizon will enforce a stabilizing control law, however, its numerical realization becomes increasingly complex. Therefore, at the core of the selection of a suitable prediction horizon there is a trade-off between short-sightedness and stabilization capabilities of the policy, and computability. This is exemplified in Figure 7, where we illustrate the role that is played by the prediction horizon in the performance of the control loop. It can be observed that a short-sighted policy with an horizon of 20 days, is less stringent in the mobility reduction, causing a larger number of hospitalised people in the long term and a larger uncertainty in the end result. Having determined that we

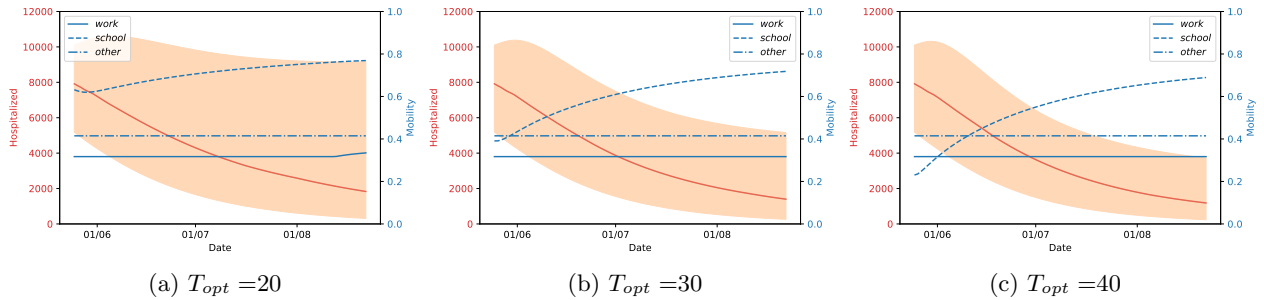


Figure 7: Dependence on optimisation window T , $(\epsilon_s, \epsilon_w, \epsilon_o) = (100, 100, 100)$ when done for $T_h = 90$ days starting on the 24th of May.

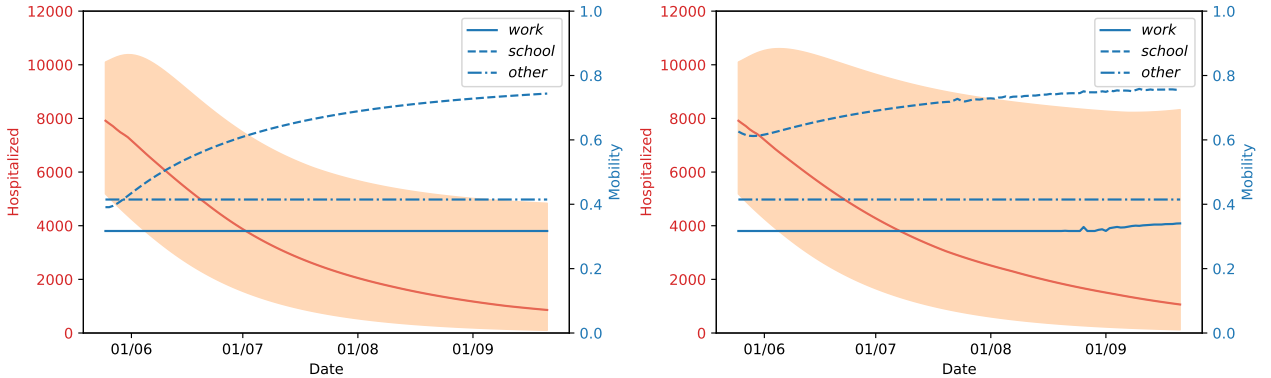
obtain similar results for control windows of $T_{opt} = 30$ and $T_{opt} = 40$ we proceed in the next subsection with this methodology using a window of $T_{opt} = 30$, which is computationally cheaper, correctly aligned with the COVID-19 time scale for transmission, and a reasonable time frame for a policy maker.

4.2 A lockdown strategy starting on the 24th of May

We now proceed to study the effect of the relative weights of each term in the cost functional. In a first moment, we assume that the economic cost of opening each type of location (school, work or others) is the same and analyse the effect of varying their relative weight to that of the sanitary cost. This is reflected in using the different values of ϵ shown in Figure 8.

The choice of suitable control penalties $\epsilon_\star, \star \in \{\text{school, work, other}\}$ is a sensitive issue in any optimal control problem. In our case, we observe that the predicted number of daily deceased at the end of the training interval is between 200 and 400 on the 23rd of May (see Figure 6). In order to show a numerical realization that is sensitive to this magnitude, having in mind that the control variables are constrained to $[0, 1]$, we scale each ϵ_\star in the order of 100.

Interestingly, we observe that for a relative weight of 100 or 200 between the economic cost and the sanitary cost, with all the ϵ_\star having the same value, all the control strategies keep m^{other} constant at a value of approximately 0.41, which is the minimum value allowed for this parameter. This behaviour is consistently reproduced for any of the values ϵ_\star that we explored as we will see below. The only situation in which we obtained a lockdown strategy that allowed for less restrictive measures on the “other” locations was by attributing a weight to the economic cost about 100 times higher than that of the sanitary cost. In this case, unsurprisingly, all the lockdown measures are lifted, with all the m^\star values converging to 1, which inevitably means the number of infected people will increase, most likely leading to a second wave of the epidemics. To understand this phenomenon we must inspect the contact matrix relative to the “other locations” category (Figure 2). It can be observed that the segment of the population on which our optimisation strategy acts, namely, the population below 60 years old, has a large number of contacts with the older segment (above 60) in that setting. As the latter are the most vulnerable to the disease, the optimisation is therefore trying to limit the number of contacts they have by reducing m^{other} .



(a) $(\epsilon_s, \epsilon_w, \epsilon_o) = (100, 100, 100)$ starting at 24th of May. (b) $(\epsilon_s, \epsilon_w, \epsilon_o) = (200, 200, 200)$ starting at the 24th of May.

Figure 8: Different relative weights between the sanitary cost and economic cost of the lockdown measures starting on the 24th of May and done for $T_h = 120$ days.

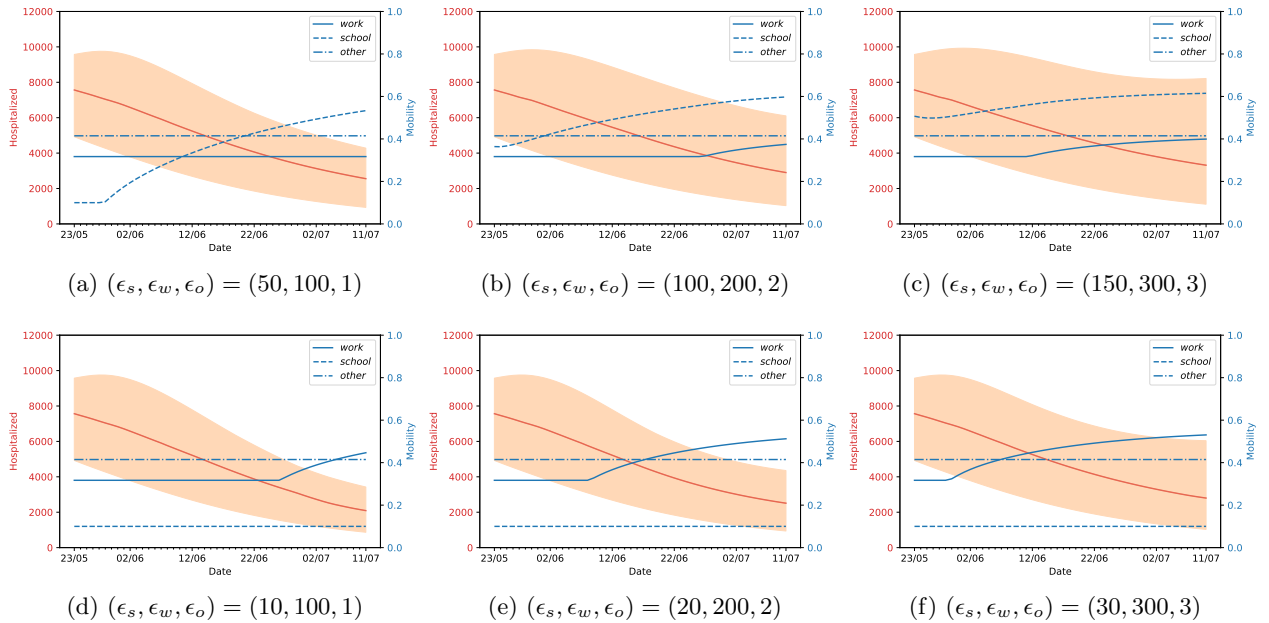


Figure 9: Different economic cost weights produce different opening strategies starting on the 24th of May and number of predicted hospitalized people.

Even though the relative weights between the sanitary and economic costs provide us with valuable information, further varying the values of ϵ_* for each category can produce a more economically viable solution. For example, opening workplaces is clearly an important part of the economy, and this might not be achievable without opening schools as well. For this reason, we will assume that closing workplaces is the measure with the highest economic cost, followed by schools and then others, and study the effects of varying the relative values of ϵ_* for each place, and the relative weight of the controls to the sanitary cost. This provides us with a variety of lockdown strategies, which we present in Figure 9.

Since the control weights ϵ_* are different in each case, we cannot compare the value of the different cost functionals directly. Hence, here we compare the strategies based on the reproduction number $\mathcal{R}(t)$ in Figure 10. Further we also compare them with the reproduction number predicted by our model if the presently observed mobility values remain at the same level as they were estimated on the 29th of May. It is

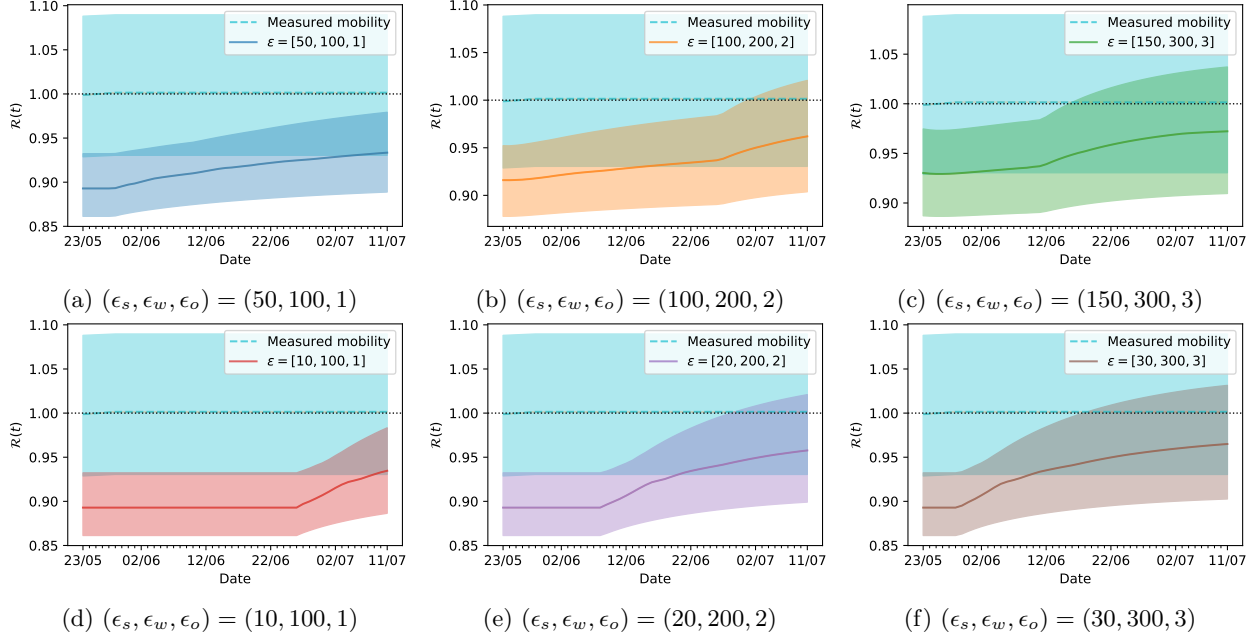


Figure 10: Evolution of $\mathcal{R}(t)$ corresponding to different opening strategies starting on the 24th of May learned using different economic cost weights for different ϵ values as in Figure 9, with 99% credibility intervals.

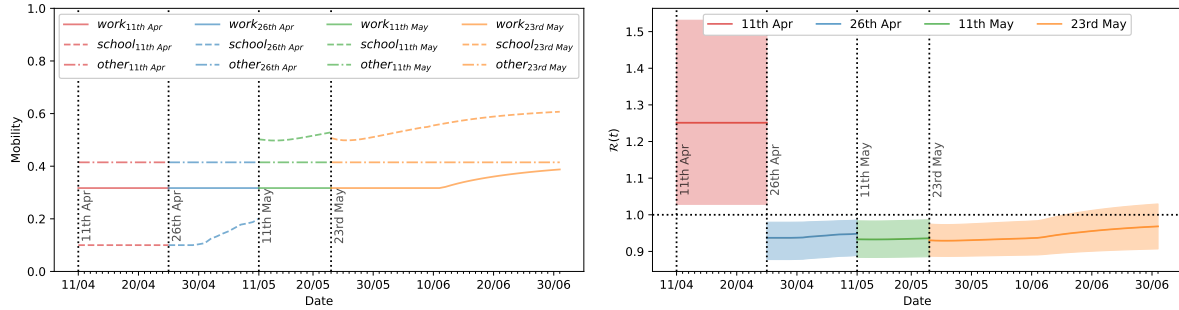
interesting to notice that the optimal strategy keeps the value of \mathcal{R} smaller than 1 for most of the optimization horizon while proposing to open workplaces and schools; it is therefore balancing in the best possible way the need to contain the epidemic and the economic cost to achieve it.

4.3 Dynamic update of the model and the optimal control strategy

As new data becomes available, we can re-perform the model fit, and obtain a new posterior distribution on the parameters to use in order to find the optimal mobility values. An instance of this *dynamic update* can be seen in Figure 11, where we show the optimal mobility values (and the corresponding basic reproduction number) after the model parameters have been fit and the optimal solution has been obtained at different observation horizons (11th of April, 26th of April, 11th of May and 23rd of May). We chose here $(\epsilon_s, \epsilon_w, \epsilon_o) = (150, 300, 3)$ as from the results in Figures 9 and 10 it can be seen that such a choice leads to an optimal control strategy that increases the mobility towards both workplaces and schools while keeping the value of $\mathcal{R}(t) < 1$.

From this experiment, we see that the optimal control strategy determined with parameter values fitted on data up to the 11th of April is extremely restrictive, as the predicted dynamics on that date badly overestimates the number of deceased and hospitalized. Instead, updating the optimal control strategy on the 26th of April results in an increase of the mobility towards schools already at the end of April. Then, on the 11th of May, the proposed optimal strategy allows schools to be open even more than what the model suggested based on data up to the 26th of April. Finally, when we reach the 26th of May, the level of schools opening is left almost unchanged, but the optimal mobility strategy determined on that date proposes to increase the mobility towards workplaces around mid-June. We also note that, with the exception of the time interval between the 11th and the 26th of April, the predicted $\mathcal{R}(t)$ value with the optimal mobility values always stays below 1. What happens in the first period of time is that the optimal strategy is as restrictive as possible, but the parameters are estimated such that even in those conditions the epidemic is predicted to increase rapidly, resulting in $\mathcal{R}(t) > 1$.

Therefore, updating the optimal control strategy iteratively allows us to rely less on long-term predictions from the model (which become more biased the farther in the future is the prediction). Together with the knowledge on model-specific biases coming from fitting the model to different horizons in the past (Section 3.2), this approach enables a policy maker to assess the validity of the proposed optimal mobility strategy and update it on a periodic basis as new data becomes available.



(a) Dynamically updated control strategy.

(b) $R(t)$ corresponding to the updated control strategies.

Figure 11: Results for the dynamically updated control strategy, as described in Section 4.3; specifically, we fit the model on data up to a given value of T_{obs} (for instance 11th April), then determine the optimal mobility strategy up to the next T_{obs} (26th April). Data until the latter is used to repeat the procedure, in order to update the optimal control strategy exploiting newly available information. In this experiment, $(\epsilon_s, \epsilon_w, \epsilon_o) = (150, 300, 3)$ is used. In panel (a), we show the optimal mobility values determined with the above strategy, with corresponding values of $R(t)$ shown in panel (b), with credibility intervals.

5 Concluding Remarks and Future Work

We have proposed an estimation/control methodology for the COVID-19 pandemic in England. Our approach is composed of the following elements: system dynamics described through an age-structured SEIR model, the use of public data such as Google Mobility for estimating model parameters, and the design of adaptive lockdown strategies in the framework of nonlinear optimal control. While the current work focused on a study of the COVID-19 pandemic in England, the underlying methodology can be extended to different spatio-temporal locations. Our systematic approach provides a computational tool to assist the design of lockdown strategies which can be periodically rectified as the model is fed with incoming public data. Moreover, the proposed strategies are parsimonious in the sense that they encode both healthcare and socio-economic factors, and realistic as they are expressed as mobility reduction parameters which can be effectively measured, as opposed to switching on-off strategies.

Arguably, our model does not capture the increase in the testing capacity. It is reasonable to assume that a larger proportion of people in the subclinical compartment get tested; ideally, these people will adhere to stringent social isolation regimes with the expectation to slow down the spread of the disease. However, how the latter affects the evolution of the epidemics when reduced mobility measures for all citizens are already in place remains unclear. As we continue to work on our approach, a natural way to improve the accuracy of our model is through a further downscaling of our dynamics, by considering 418 principal local authorities (LA) in the UK, along with a commuting network of UK citizens between them constructed from the 2011 census data. Such a refined model, whose numerical treatment will necessarily require the use of high-performance computing resources, would allow the design of space-time adaptive lockdowns. Our progress along these lines will be documented on the companion website¹¹.

References

G. Albi, M. Bongini, E. Cristiani, and D. Kalise. Invisible control of self-organizing agents leaving unknown environments. *SIAM Journal on Applied Mathematics*, 76(4):1683–1710, 2016. doi: 10.1137/15M1017016.

G. Albi, L. Pareschi, and M. Zanella. Control with uncertain data of socially structured compartmental epidemic models. *arXiv preprint arXiv:2004.13067*, 2020.

R. M. Anderson and R. M. May. *Infectious diseases of humans: dynamics and control*. Oxford university press, 1992.

¹¹ <https://optimallockdown.github.io/Covid19inEngland/>

R. Bailo, M. Bongini, J. A. Carrillo, and D. Kalise. Optimal consensus control of the cucker-smale model. *IFAC-PapersOnLine*, 51(13):1 – 6, 2018.

M. A. Beaumont. Approximate bayesian computation in evolution and ecology. *Annual review of ecology, evolution, and systematics*, 41:379–406, 2010.

A. Charpentier, R. Elie, M. Laurière, and V. C. Tran. Covid-19 pandemic control: balancing detection policy and lockdown intervention under icu sustainability. *arXiv preprint arXiv:2005.06526*, 2020.

M. Chinazzi, J. T. Davis, M. Ajelli, C. Gioannini, M. Litvinova, S. Merler, A. P. y Piontti, K. Mu, L. Rossi, K. Sun, et al. The effect of travel restrictions on the spread of the 2019 novel coronavirus (covid-19) outbreak. *Science*, 368(6489):395–400, 2020.

N. G. Davies, P. Klepac, Y. Liu, K. Prem, M. Jit, R. M. Eggo, C. C.-. working group, et al. Age-dependent effects in the transmission and control of covid-19 epidemics. *MedRxiv*, 2020.

R. Dutta, M. Schoengens, J.-P. Onnela, and A. Mira. Abcpy: A user-friendly, extensible, and parallel library for approximate bayesian computation. In *Proceedings of the Platform for Advanced Scientific Computing Conference*, pages 1–9, 2017.

M. Gatto, E. Bertuzzo, L. Mari, S. Miccoli, L. Carraro, R. Casagrandi, and A. Rinaldo. Spread and dynamics of the covid-19 epidemic in italy: Effects of emergency containment measures. *Proceedings of the National Academy of Sciences*, 117(19):10484–10491, 2020.

L. Grüne and J. Pannek. Nonlinear model predictive control. In *Nonlinear Model Predictive Control*, pages 45–69. Springer, 2017.

J. Hilton and M. J. Keeling. Estimation of country-level basic reproductive ratios for novel coronavirus (covid-19) using synthetic contact matrices. *medRxiv*, 2020.

IHME and C. J. Murray. Forecasting covid-19 impact on hospital bed-days, icu-days, ventilator-days and deaths by us state in the next 4 months. *MedRxiv*, 2020.

W. O. Kermack and A. G. McKendrick. A contribution to the mathematical theory of epidemics. *Proceedings of the royal society of london. Series A, Containing papers of a mathematical and physical character*, 115 (772):700–721, 1927.

P. Klepac, A. J. Kucharski, A. J. Conlan, S. Kissler, M. Tang, H. Fry, and J. R. Gog. Contacts in context: large-scale setting-specific social mixing matrices from the bbc pandemic project. *medRxiv*, 2020.

A. J. Kucharski, T. W. Russell, C. Diamond, Y. Liu, J. Edmunds, S. Funk, R. M. Eggo, F. Sun, M. Jit, J. D. Munday, et al. Early dynamics of transmission and control of covid-19: a mathematical modelling study. *The lancet infectious diseases*, 2020.

J. Lintusaari, M. U. Gutmann, R. Dutta, S. Kaski, and J. Corander. Fundamentals and recent developments in approximate bayesian computation. *Systematic biology*, 66(1):e66–e82, 2017.

K. Prem, A. R. Cook, and M. Jit. Projecting social contact matrices in 152 countries using contact surveys and demographic data. *PLoS computational biology*, 13(9):e1005697, 2017.

K. Prem, Y. Liu, T. W. Russell, A. J. Kucharski, R. M. Eggo, N. Davies, S. Flasche, S. Clifford, C. A. Pearson, J. D. Munday, et al. The effect of control strategies to reduce social mixing on outcomes of the covid-19 epidemic in wuhan, china: a modelling study. *The Lancet Public Health*, 2020.

T. Rawson, T. Brewer, D. Veltcheva, C. Huntingford, and M. Bonsall. How and when to end the covid-19 lockdown: an optimisation approach. *Frontiers in Public Health*, 2020.

C. Rothe, M. Schunk, P. Sothmann, G. Bretzel, G. Froeschl, C. Wallrauch, T. Zimmer, V. Thiel, C. Janke, W. Guggemos, et al. Transmission of 2019-ncov infection from an asymptomatic contact in germany. *New England Journal of Medicine*, 382(10):970–971, 2020.

A. Savitzky and M. J. Golay. Smoothing and differentiation of data by simplified least squares procedures. *Analytical chemistry*, 36(8):1627–1639, 1964.

E. Trélat and E. Zuazua. The turnpike property in finite-dimensional nonlinear optimal control. *Journal of Differential Equations*, 258(1):81 – 114, 2015. ISSN 0022-0396. doi: <https://doi.org/10.1016/j.jde.2014.09.005>. URL <http://www.sciencedirect.com/science/article/pii/S0022039614003568>.

P. Virtanen, R. Gommers, T. E. Oliphant, M. Haberland, T. Reddy, D. Cournapeau, E. Burovski, P. Peterson, W. Weckesser, J. Bright, et al. Scipy 1.0: fundamental algorithms for scientific computing in python. *Nature methods*, 17(3):261–272, 2020.

D. J. Warne, A. Ebert, C. Drovandi, A. Mira, and K. Mengersen. Hindsight is 2020 vision: Characterisation of the global response to the covid-19 pandemic. *medRxiv*, 2020.

Y. Xiang and X. Gong. Efficiency of generalized simulated annealing. *Physical Review E*, 62(3):4473, 2000.

A Inference on data until 23rd of May

A.1 Deaths for each age group

In Figure 12 we report the median and 99 percentile credibility interval of the daily deceased in each of the 5 age groups, and we compare it to the actual data (green). Note that the credibility interval is larger for age groups 1 and 2; this is expected, as the number of deaths in that age groups is relatively small, so that achieving a good fit is harder. Moreover, we also report the cumulative deaths over the different age groups in Figure 13.

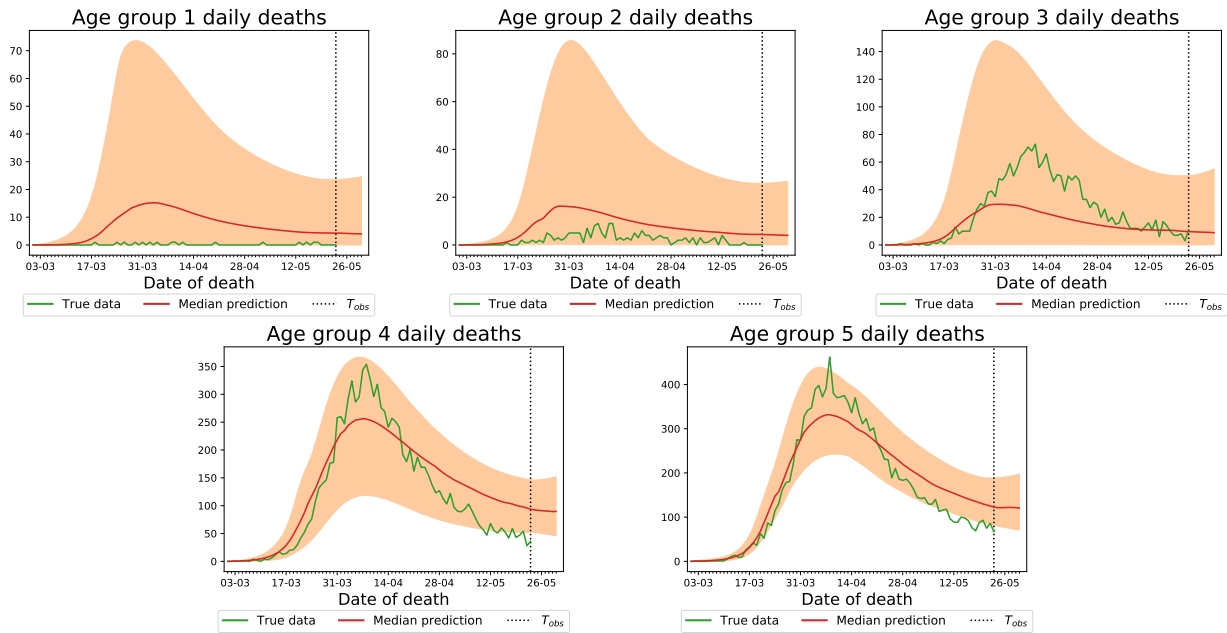


Figure 12: Comparison of number of daily deceased predicted by our model and actual one (green line), for each age group.

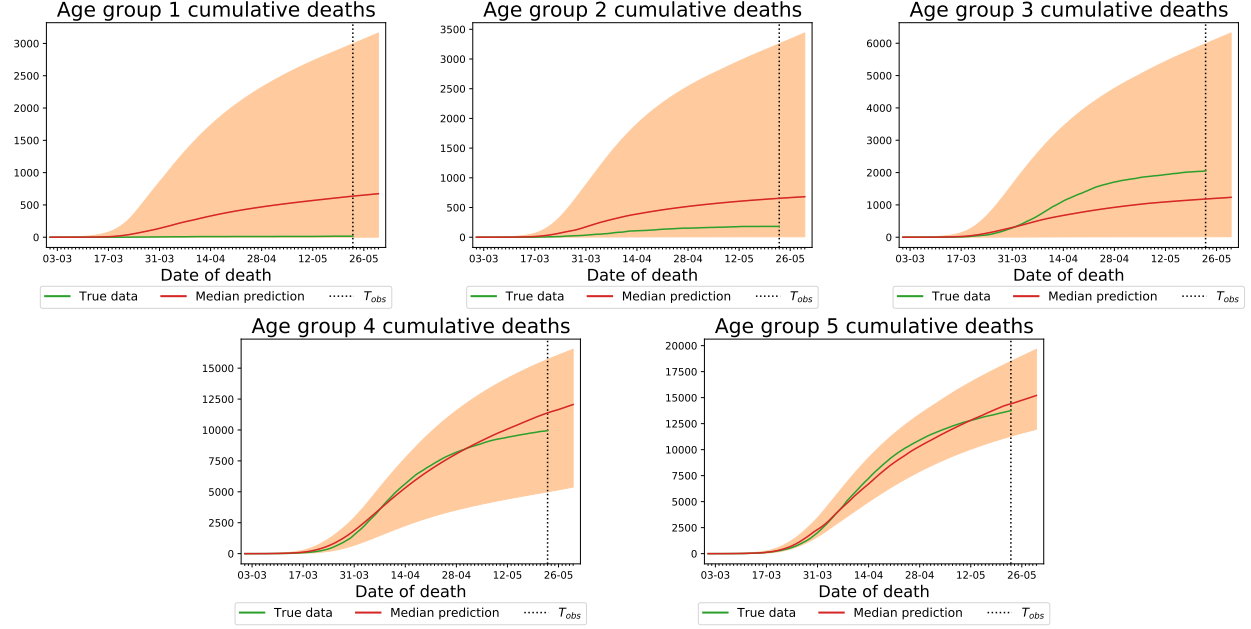


Figure 13: Comparison of cumulative deaths predicted by our model and actual one (green line), for each age group. Note that the number of deaths in Age Group 1 is very much overestimated by our model. This is due to the relatively small number of deaths in that age group, which make it hard to obtain a good fit.

A.2 Additional results on latent variables

We report here the inferred evolution of the unobserved compartments.

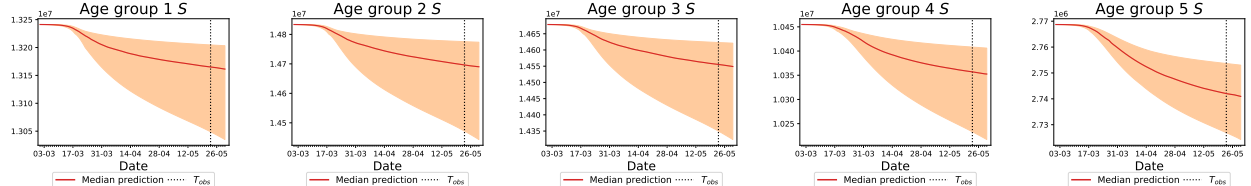


Figure 14: Inferred Susceptible population.

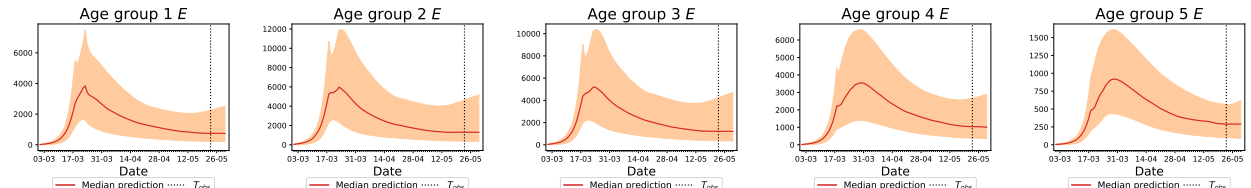


Figure 15: Inferred Exposed population.

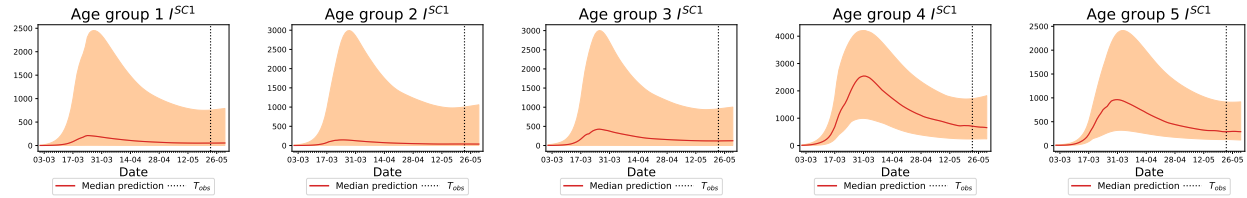


Figure 16: Inferred Infected SubClinical 1 population.

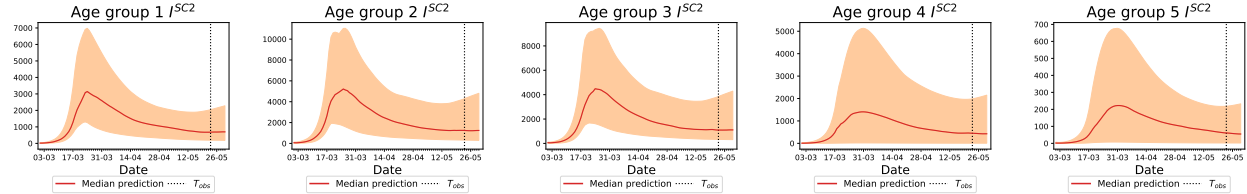


Figure 17: Inferred Infected SubClinical 2 population.

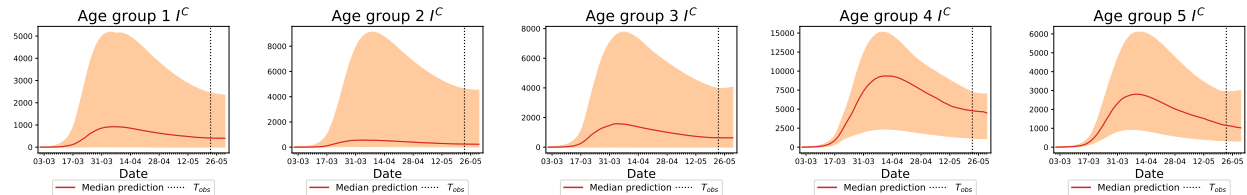


Figure 18: Inferred Infected Clinical population.

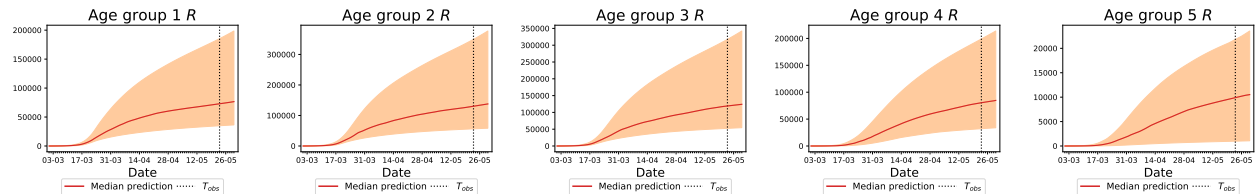


Figure 19: Inferred Removed population.

B Additional plots on posterior distribution with inference on data until 23rd of May

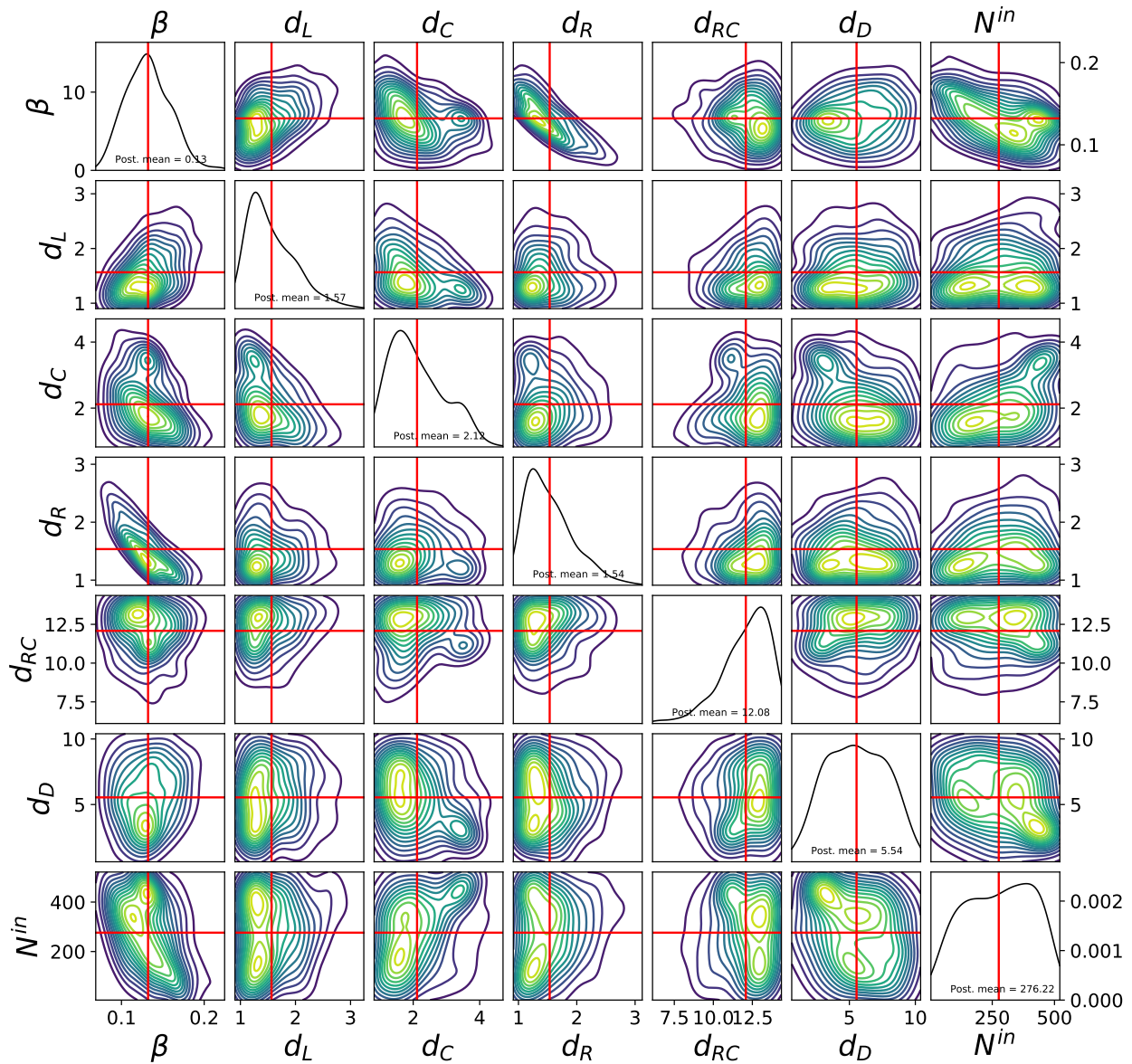


Figure 20: Single and bivariate marginals for the parameters describing the transition between states; note for instance the negative correlation between β and d_R ; this is expected from the dynamics of the model (the longer a person stay in the infectious state, the more people can infect; therefore, a similar dynamics can be obtained by a lower value of β).

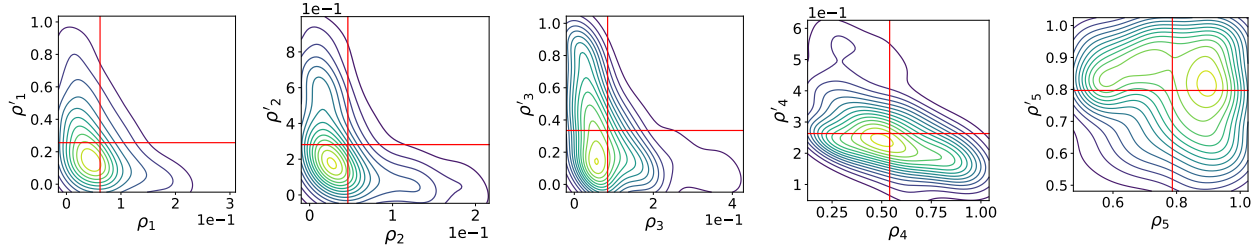


Figure 22: Bivariate posterior plots for ρ_i and ρ'_i , for all age groups ($i = 1, \dots, 5$). For all of them, some negative correlation is present; this is very evident in the case of age group 4.

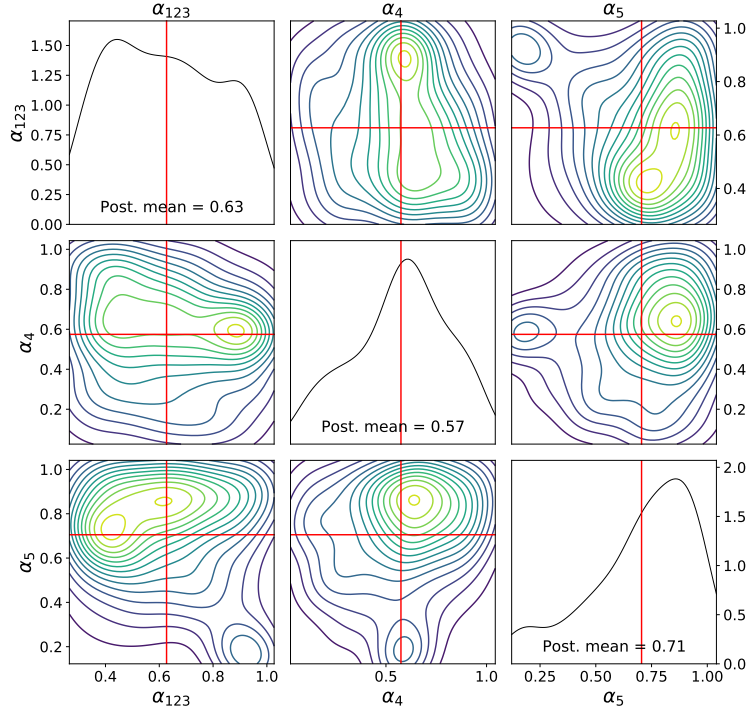


Figure 23: Single and bivariate marginals for the parameters connecting the reduction in mobility to the change of social contacts.

C Additional plots on optimal control using training data until 11th of May

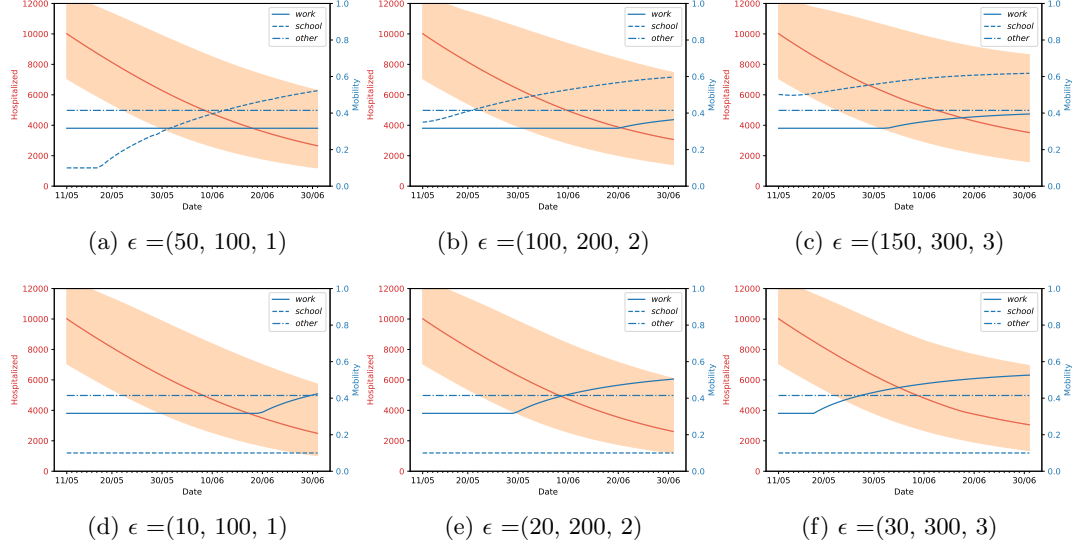


Figure 24: Different economic cost weights produce different opening strategies and number of predicted hospitalized people.

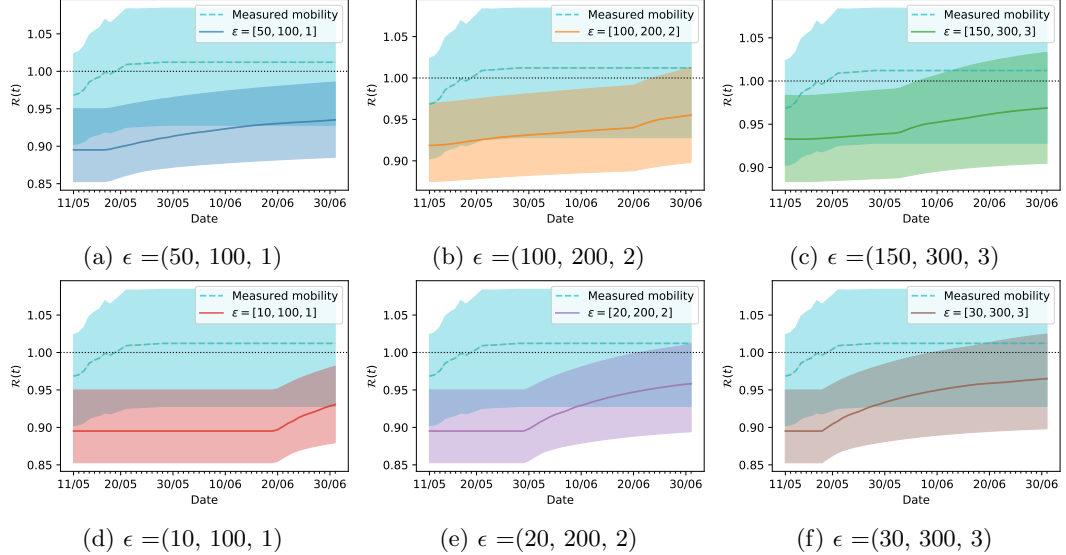


Figure 25: Evolution of $\mathcal{R}(t)$ for different ϵ values, with 99% credibility intervals, for optimal mobility values compared with measured mobility values (observed until the 29th of May and assumed constant thereafter).